Environmental Science & Technology

pubs.acs.org/est

Article

Formation Mechanisms and Source Apportionments of Airborne Nitrate Aerosols at a Himalayan-Tibetan Plateau Site: Insights from Nitrogen and Oxygen Isotopic Compositions

Yu-Chi Lin, Yan-Lin Zhang,* Mingyuan Yu, Mei-Yi Fan, Feng Xie, Wen-Qi Zhang, Guangming Wu, Zhiyuan Cong, and Greg Michalski

Cite This: *Environ. Sci. Technol.* 2021, 55, 12261−12271

Read Online

ACCESS | Metrics & More | Article Recommendations | Supporting Information

ABSTRACT: Formation pathways and sources of atmosphere nitrate (NO_3^-) have attracted much attention as NO_3^- had detrimental effects on Earth's ecosystem and climate change. Here, we measured nitrogen ($\delta^{15}N\text{-}NO_3^-$) and oxygen ($\delta^{18}O\text{-}NO_3^-$ and $\Delta^{17}O\text{-}NO_3^-$) isotope compositions in nitrate aerosols at the Qomolangma station (QOMS) over the Himalayan-Tibetan Plateau (HTP) to quantify the formation mechanisms and emission sources of nitrate at the background site. At QOMS, the enhanced NO_3^- concentrations were observed in the springtime. The average $\delta^{15}N\text{-}NO_3^-$, $\delta^{18}O\text{-}NO_3^-$, and $\Delta^{17}O\text{-}NO_3^-$ values were 0.4 ± 4.9, 64.7 ± 11.5 and 27.6 ± 6.9‰, respectively. Seasonal variations of isotope ratios at QOMS can be explained by the different emissions and formation pathways to nitrate. The average fractions of NO_2 + OH and N_2O_5 + H_2O to nitrate production were estimated to be 43 and 52%, respectively, when the NO_3 + hydrocarbon (HC)/dimethyl sulfide (DMS) (NO_3 + HC/DMS) pathway was assumed to be 5%. Using stable isotope analysis in the R (SIAR) model, the relative contributions of biomass burning (BB), biogenic soil emission, traffic, and coal combustion to nitrate were estimated to be 28, 25, 24, and 23%, respectively, on yearly basis. By FLEXible PARTicle (FLEXPART) dispersion model, we highlighted that NO_x from BB emission over South Asia that had undergone N_2O_5 + H_2O processes enhanced the nitrate concentrations in the springtime over the HTP region.

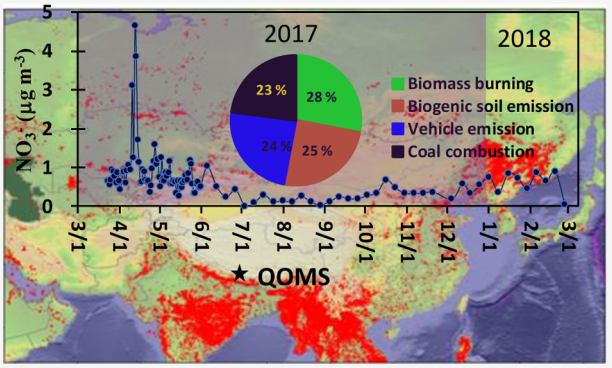

KEYWORDS: *nitrate aerosols, nitrogen and oxygen isotopes, Himalayan-Tibetan Plateau, formation pathways, biomass burning*

INTRODUCTION

Nitrate (NO_3^-), a terminal species in nitrogen cycles, constitutes a major fraction of ambient particulate matter (PM). Nitrate enhances its cloud-droplet nucleating ability and also increases the cloud-drop number concentrations as well as cloud albedo, leading to indirect influences on Earth's climate.[1,2] In the atmosphere, nitrate aerosols are mainly produced by the transformation of NO_x through three different pathways: (1) NO_2 oxidation by OH (NO_2 + OH) in the gas phase, (2) hydrolysis of N_2O_5 on preexisting aerosols (N_2O_5 + H_2O, heterogeneous process), and (3) reaction between NO_3 radicals and hydrocarbons (HC)/dimethyl sulfide (DMS) (NO_3 + HC/DMS herein). The latter two mechanisms mainly occur at nighttime, and hence, these reactions are also called "nocturnal chemistry".[3] On a global scale, the contribution (41%) of NO_2 + OH to nitrate was equal to that of N_2O_5 + H_2O in the troposphere below 1 km altitude, while NO_3 + HC/DMS contributed a minor fraction (~5%) of nitrate formation.[4]

Formation mechanisms and source apportionments of nitrate aerosols have attracted more attention over China in recent years. In urban cities, NO_3^- was mainly formed by secondary transformation of NO_x from local and regional emissions.[5,6] Under specific atmospheric conditions, NO_3^- concentrations exceeded dozens of μg m^{-3}, inducing PM haze formation and threatening human health.[5,6] Thus, studies of source apportionments and formation pathways of nitrate at urban sites would be important to realize the evolution of haze formation and to take control measures for alleviation of haze events. Unlike urban cities, NO_3^- at background sites was at a low level (~1 μg m^{-3}) and was profoundly from regional transport. The NO_3^- data at background sites would provide

Received: June 17, 2021
Revised: August 10, 2021
Accepted: August 20, 2021
Published: September 1, 2021

https://doi.org/10.1021/acs.est.1c03957
Environ. Sci. Technol. 2021, 55, 12261−12271

valuable information for model studies on long-range-transported pollution and on the response of climate change to regional air pollutant emissions.[7]

The isotope technique is a good tool to track potential sources and formation pathways of atmospheric nitrate aerosols. NO_x originating from various emission sources possesses unique features of nitrogen isotope ratios. Using isotope signatures combined with the isotope mixing model, source apportionments of gaseous NO_x and particulate NO_3^- can be quantified.[6,8,9] Oxygen isotopic compositions, such as $\delta^{18}O$ and oxygen-17 anomaly ($\Delta^{17}O$) in nitrate, were commonly used to investigate the formation mechanisms of nitrate aerosols.[6,10,11] Due to the different contributions of $\delta^{18}O$ in nitrate aerosols ($\delta^{18}O\text{-}NO_3^-$) from O_3, the $\delta^{18}O\text{-}NO_3^-$ values from NO_2 + OH and the hydrolysis of N_2O_5 are significantly distinct. Hastings et al.[12] reported that $\delta^{18}O\text{-}NO_3^-$ from NO_2 + OH had two-thirds of contribution from O_3, whereas $\delta^{18}O\text{-}NO_3^-$ from the hydrolysis of N_2O_5 possessed five-sixth of contribution from O_3. This led to more enriched $\delta^{18}O\text{-}NO_3^-$ and $\Delta^{17}O$ in nitrate aerosols ($\Delta^{17}O\text{-}NO_3^-$) produced by the N_2O_5 + H_2O process.[10] Using this feature, the formation pathways of nitrate aerosols have been quantified in urban and background areas.[6,10,13,14]

Owing to a large area covered by glaciers, the Himalayan-Tibetan Plateau (HTP) region is referred to as the "Third Pole" and "Water Tower of Asia", serving as a water reservoir for the Asian ecosystem and human survival. Previously, several studies have characterized atmospheric aerosols and identified their potential sources in the HTP region.[7,14−19] Most of these studies were focused on black carbon (BC) since it is an important species for atmospheric heating, melting the Himalayan glaciers and resulting in flood disasters for the neighboring countries.[20] However, only a few studies have mentioned nitrate concentrations in the HTP region.[7,14] For instance, Zhao et al.[7] found that the average NO_3^- concentration at Qinghai Lake (northeastern margin of the HTP) during the springtime was 3.3 $\mu g\ m^{-3}$, which was 1.2−2.5 times higher than those in other seasons. At Qomolangma station (QOMS, the sampling site of this work), the enhanced nitrate concentrations were also found in springtime.[14] Using the isotope techniques, they suggested that vehicle exhaust and agriculture activities played a dominant role in contributing nitrate aerosols at this mountain site. Although some studies characterized nitrate in the HTP region, the formation pathways and source apportionments of nitrate in the HTP region were not well quantified, especially during the high nitrate-level season (springtime). In this work, the total suspended particulate (TSP, aerodynamic diameter less than 100 μm) samples were collected at QOMS from March 2017 to February 2018. Apart from water-soluble inorganic ions, the nitrogen isotope compositions in nitrate ($\delta^{15}N\text{-}NO_3^-$), $\delta^{18}O\text{-}NO_3^-$, and $\Delta^{17}O\text{-}NO_3^-$ were also analyzed. Here, we reported the nitrate concentrations and their accompanying $\delta^{15}N\text{-}NO_3^-$, $\delta^{18}O\text{-}NO_3^-$, and $\Delta^{17}O\text{-}NO_3^-$ values at QOMS. Using a Bayesian isotope mixing model and the FLEXible PARTicle (FLEXPART) dispersion model, the formation pathways and potential sources together with source regions of nitrate aerosols at OQMS would be quantified.

MATERIALS AND METHODS

Aerosol Sampling. Airborne TSP samples were collected at QOMS (28.36°N, 86.95°E, 4276 m a.s.l., see Figure S1), which is located in a dry valley with complex terrain and is about 30 km north of Mt. Everest (8844 m a.s.l.). QOMS was established for routine monitoring of the atmospheric environment over the HTP region in August 2005.[21] It also belonged to the monitoring network of atmospheric pollution and cryospheric changes,[20] and the TSP sampling frequency was normally from 3 to 7 days.[14,20] In this work, TSP samples were collected at QOMS from March 2017 to February 2018, with a frequency of 7 days, except for the springtime (a frequency of 1 day) when high concentrations of particle compositions were regularly found during the South Asian biomass burning (BB) period.[14,15] The high frequency of TSP sampling in the springtime was to explore the formation pathways and emission sources of nitrate aerosols under the high nitrate-level conditions. During the sampling period, each aerosol sample was collected from 10:30 local time (LT) to 10:00 LT on the next day, using a high-volume TSP sampler (TISCH, model TE-5170D), which was operated at a flow rate of approximately 1.1 $m^3\ min^{-1}$. Quartz filters (8 in. × 10 in., PALL) were used as filtration substrates. Prior to sampling, each filter was heated at 450 °C for 4.5 h to remove impurities in the filter. After sampling, each filter was folded and stored in a separate plastic bag, which was then stored in a polypropylene container, frozen immediately, and returned to the laboratory for further chemical analyses.

Ionic Species Analysis. After sampling, two punched sampled filters (~4.02 cm^2) were extracted with 15 mL of Milli-Q water (18.2 Ω) for 30 min. After removal of insoluble particles using membrane filters (0.22 μm), the extracted solution was then analyzed for ionic species, such as Cl^-, NO_3^-, SO_4^{2-}, Na^+, NH_4^+, K^+, Mg^{2+}, and Ca^{2+}, by ion chromatography (IC, ICS5000+, Thermo Scientific). A quality assurance/quality control (QA/QC) program for analyzed ions, such as recovery and precision test along with method detection limits (MDLs), was conducted during the analyzed procedures. A multi-ion solution (Merck) was used for making a seven-point calibration curve of the IC instrument for each batch of chemical analysis. On average, the MDL for nitrate was 0.08 $\mu g\ m^{-3}$ and was from 0.03 $\mu g\ m^{-3}$ for Cl^- to 0.41 $\mu g\ m^{-3}$ for Ca^{2+}. The recoveries of all ions ranged from 90 to 110% and the precision was less than 2%. The details of this method can be found elsewhere.[22]

Isotope Analysis. For isotope analysis, the aerosol samples collected in the springtime were analyzed with $\delta^{15}N\text{-}NO_3^-$, $\delta^{18}O\text{-}NO_3^-$, and $\Delta^{17-}NO_3^-$ values to investigate the formation mechanisms and potential sources of enhanced nitrate concentrations during the South Asian BB period. In addition, we also selected some aerosol samples in other seasons for isotope analysis. This provided the comparisons of formation mechanisms and source apportionments of nitrate between the springtime and other seasons. The nitrogen and oxygen isotopic compositions in nitrate aerosols were analyzed with a bacterial denitrifier method.[23−25] Briefly, a small piece (2.54 cm^2) of sampled filter (≥0.8 μgN) was extracted with 5 mL of Milli-Q water (18.2 Ω) for 30 min and insoluble particles were then filtered by membrane filters (0.22 μm). Further, NO_3^- in the extracted solution was converted to N_2O by *Pseudomonas aureofaciens* (ACTT# 13985), which has no N_2O-reductase activity. The produced N_2O was subsequently decomposed into N_2 and O_2 in a gold tube at a temperature of 800 °C. After that, the produced N_2 and O_2 were analyzed with ^{14}N, ^{15}N, ^{16}O, ^{17}O, and ^{18}O by an isotope ratio mass spectrometer (MAT253, Thermo Fisher Scientific) with a multipurpose online preparation device (GasBench) and a trace gas

https://doi.org/10.1021/acs.est.1c03957
Environ. Sci. Technol. 2021, 55, 12261−12271

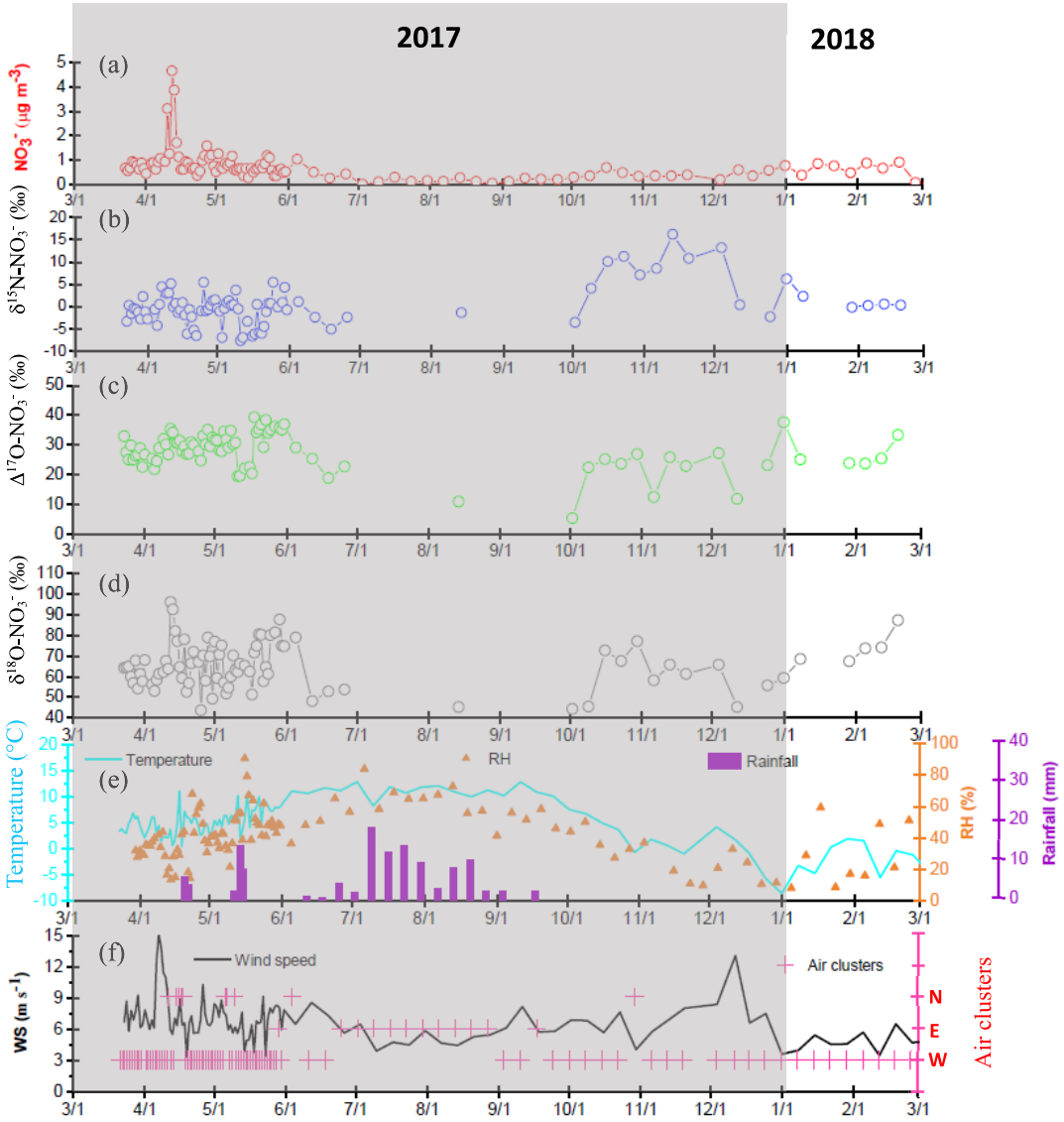

Figure 1. Time series of (a) NO_3^- concentrations, (b) δ^{15}N-NO_3^-, (c) Δ^{17}N-NO_3^-, (d) δ^{18}O-NO_3^-, (e) ambient temperature, relative humidity (RH) together with rainfall, and (f) wind speed and air clusters at QOMS during the sampling period. The shaded part represents the year 2017.

preconcentration device (Precon, at 21 °C). In this process, high purity of xenon gas (99.99%, Air Liquid, China) was used as a carrier gas. Using the results of ^{14}N, ^{15}N, ^{16}O, ^{17}O, and ^{18}O, δ^{15}N, δ^{18}O, and Δ^{17}O can then be obtained (see Supporting Information S1). During the isotope analysis, the international nitrate standards, such as USGS34, USGS35, and IAEA-NO_3^-, were used for data calibration. Based on replicate measurements of the international nitrate standards, the uncertainties of δ^{15}N, δ^{18}O, and Δ^{17}O were 0.2, 0.3, and 0.2‰, respectively. The details of this method can be found elsewhere.[25,26]

Stable Isotope Analysis in the R (SIAR) Model. The stable isotope analysis in the R (SIAR) model, which has been widely used to estimate the source apportionments of atmospheric nitrate,[6,22,27] was employed to quantify the emission sources of nitrate aerosols at QOMS. Using the SIAR model, the probability distributions of source contributions to a mixture and the uncertainty associated with multiple sources can be determined.[28] The principle of the SIAR model can be found in Supporting Information S2. To quantify the potential sources of nitrate aerosols, the δ^{15}N-NO_3^- values in ambient samples and δ^{15}N values in NO_x (δ^{15}N-NO_x) from various emission sources must serve as input in the SIAR model. Here, the δ^{15}N-NO_x values of emission sources were obtained from those reported in the literature studies.[29−39] Vehicle emission and coal combustion are well-known important sources of atmospheric NO_x.[40,41] In addition, BB (e.g., open burning for agricultural waste and weeds to obtain land for sowing) and biogenic soil emission also contributed a part of atmospheric NO_x.[39,41] Consequently, four emission sources mentioned above were considered in apportioning the emission sources of nitrate aerosols at QOMS. Table S1 lists the δ^{15}N-NO_x values in the four emission sources used in the current study. The δ^{15}N-NO_x values of coal combustion, vehicle emission, BB, and biogenic soil emission were set to be 13.7 ± 4.6, −6.6 ± 7.1, 1.1 ± 3.8, and −31.6 ± 10.1‰, respectively, in the SIAR model. Using these δ^{15}N-NO_x values, the source apportionments of nitrate aerosols at QOMS would be quantified.

As reported by Parnell et al.,[28] the SIAR model worked exceptionally well for numerous data sets ($N \geq 10$) of input of ambient δ^{15}N-NO_3^- values. Also, the ambient samples serving

https://doi.org/10.1021/acs.est.1c03957
Environ. Sci. Technol. 2021, 55, 12261−12271

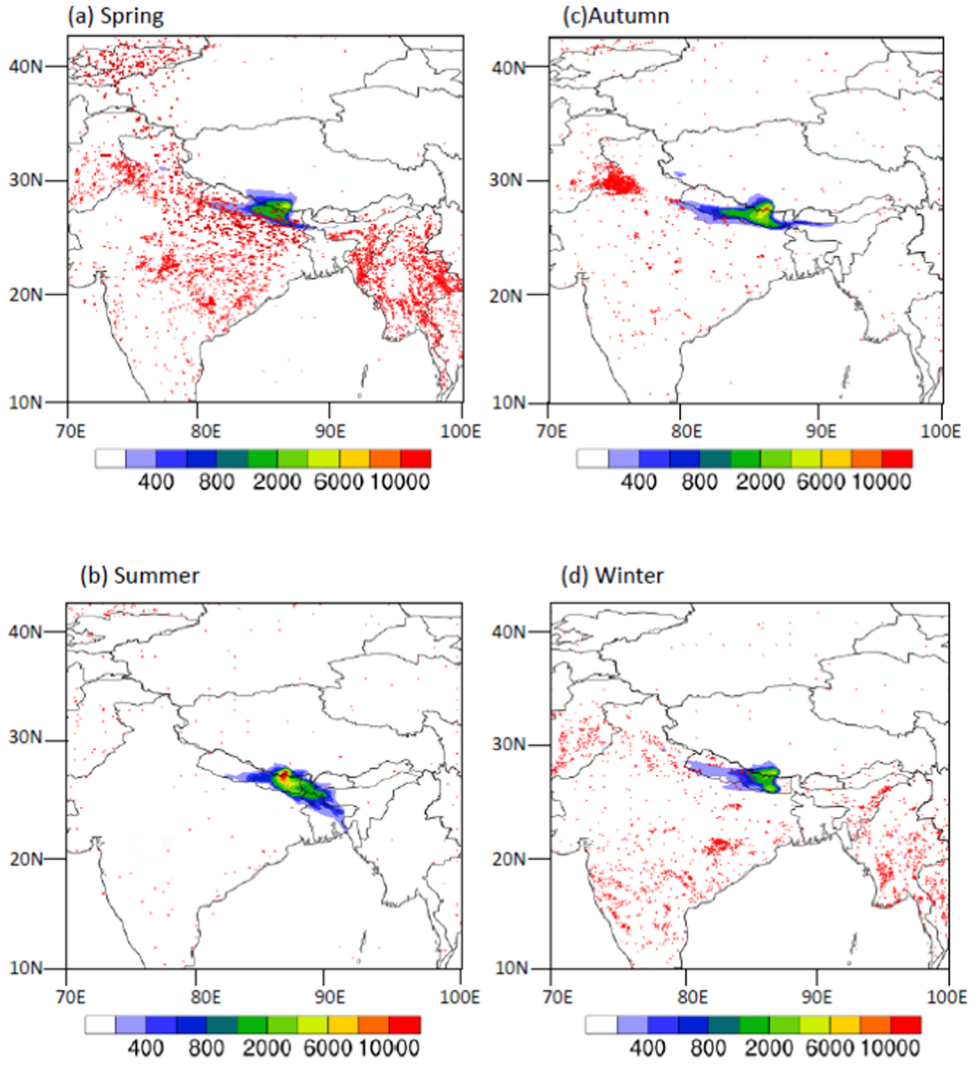

Figure 2. Footprints of nitrate aerosols using the FLEXPART model in the (a) spring, (b) summer, (c) autumn, and (d) winter. The color scale denotes the residence time (s) of nitrate aerosols in the grid cell. The red dots represent fire spots observed by the MODIS and can be downloaded from https://firms.modaps.eosdis.nasa.gov/download/.

as input should have the same nature attributes, eliminating the uncertainty caused by the different attributes between the different input data, such as the different δ^{15}N-NO_3^- values between the different seasons.[6] Therefore, we classified our observed δ^{15}N-NO_3^- data into four different groups based on the samples collected in different seasons, and the data sizes of δ^{15}N-NO_3^- were 62, 6, 9, and 9 in the spring, summer, autumn, and winter, respectively. Each data group served as one input for the SIAR model to quantify the emission sources of nitrate aerosols at QOMS in different seasons.

Hybrid Single-Particle Lagrangian Integrated Trajectory (HYSPLIT) and FLEXPART Models. To realize the influence of transported routes of the air parcels on the chemical compositions and isotope ratios in aerosol samples, 3-day backward trajectories at QOMS were computed by hybrid single-particle Lagrangian integrated trajectory (HYSPLIT) model developed by the USA NOAA Air Resources Laboratory.[42] The Global Data Assimilation System (GDAS) processed by the National Centers for Environmental Prediction (NCEP) was used for meteorological data to obtain the trajectories. During the sampling period, the backward trajectory of each sampling day was computed at 12:00 LT with an altitude of 4500 m. A total of 106 backward trajectories were acquired and further categorized into three different air groups, namely, W, N, and E air clusters, according to their originated regions and transported routes (see Figure S1). In brief, the air parcels of the W category (~78% of the total air parcels) mainly originated from Afghanistan, passing over Pakistan, northwestern/northern India, and Nepal, and then arrived at the receptor site. The air masses of the N group (~9%) mainly originated from Uzbekistan, crossing over northwestern and western China (Xinjiang and Tibet) before arriving at the sampling site. The air masses of E cluster (~13%) profoundly came from southeast Asia, crossing over northern India and Nepal before arriving at the QOMS.

Moreover, the FLEXPART model (version 10.4) was employed to identify the potential source regions of aerosols at QOMS. Previously, the FLEXPART model has been successfully used to identify the footprints of atmospheric aerosols and gaseous pollutants at both urban and high mountain sites.[43−45] The details of the FLEXPART model can be found elsewhere.[46] In this work, the meteorological data used to drive the FLEXPART model was from NCEP-FNL datasets. The spatial resolution of the model was 0.2° × 0.2°.

https://doi.org/10.1021/acs.est.1c03957
Environ. Sci. Technol. 2021, 55, 12261−12271

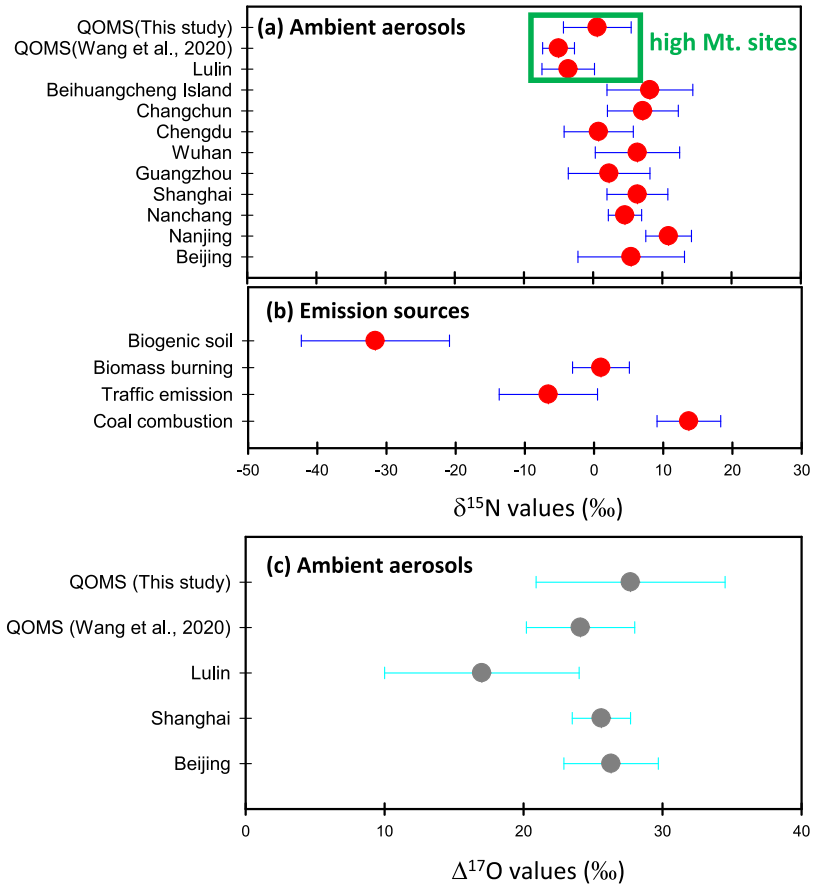

Figure 3. (a) δ^{15}N-NO_3^- values at various sampling sites, (b) δ^{15}N-NO_x values from different emission sources, and (c) Δ^{17}O-NO_3^- values at various sampling sites. The δ^{15}N-NO_3^- and Δ^{17}O -NO_3^- values in various cities were obtained from Zong et al.,[27] Chang et al.,[9] He et al.,[10] Luo et al.,[13] Wang et al.,[14] Zhao et al.,[26] and Guha et al.[51] The δ^{15}N-NO_x values are depicted in the references listed in Table S1.

For each aerosol sampling day, 10 000 particles were released every 6 h (0:00, 6:00, 12:00, and 18:00 LT) from the sampling site and then tracked backward in time for 72 h. The residence times of all particles in a depth of 1000 m above the ground were recorded to obtain the footprints.

RESULTS AND DISCUSSION

Overview of Nitrate Concentrations. During the sampling period, the daily ambient temperature varied from −8.5 to 12.9 °C and the relative humidity (RH) ranged from 8 to 91%. As expected, cold-dry air was frequently found in the winter and warm-wet air was observed in the summer (see Figure 1). Intensive rainfall was observed in the summertime. A total of 106 TSP samples were collected at QOMS during the sampling period. Due to a large uncertainty of gravimetric weighting for quartz filters, the TSP mass concentrations were not obtained. The concentrations of the total water-soluble inorganic ions (TWSIIs) at QOMS varied from 0.2 to 14.0 μg m^{-3} with a mean value of 3.5 ± 2.2 μg m^{-3}. The significant seasonal variations of TWSIIs were observed, with a maximum in the spring (4.2 μg m^{-3}) and a minimum in the summer (1.3 μg m^{-3}, Table S2). This seasonality was in agreement with that over the HTP region in an earlier study.[19] The high TWSIIs concentration in the spring was associated with the BB emission in South Asia, while the lower TWSIIs level in the summer might be attributed to the increasing rainfall to wash out the atmospheric particles (Figure 1e).[19] In addition, much fewer fire spots over South Asia in the summer (Figure 2) might also lower the TWSIIs concentrations. At QOMS, sulfate was the most predominant species, accounting for 37% of the TWSIIs mass, followed by Ca^{2+} (27%), NO_3^- (20%), and NH_4^+ (10%) (see Figure S2). The high concentrations of Ca^{2+} at this mountain site (except for the summer, see Figure S3) suggested that fugitive dust was also a dominant source of TSP at QOMS. No significant difference in the relative fraction of each ion to TWSIIs was found in the distinct air clusters (Figure S2). However, the absolute TWSIIs concentrations were different in the distinct air groups with the highest concentration (5.2 μg m^{-3}) in the N air cluster and the lowest level (0.9 μg m^{-3}) in the E air category. During the sampling period, the E air cluster was chiefly found in the summer (Figure 1f), and therefore, the lower TWSIIs concentration in this air category would be expected. The N air cluster was profoundly found in the springtime when the intensive fire spots were observed in Uzbekistan, Kyrgyzstan, and northwestern Xinjiang, China (see Figure 2a). The air masses originating and crossing these regions might pick up the BB pollution and transport it to the receptor site and enhance the TWSIIs concentrations.

The daily NO_3^- concentrations at QOMS varied from <0.1 to 4.7 μg m^{-3} (Figure 1a), with a mean value of 0.7 ± 0.6 μg m^{-3}. As shown in Figure S4, the equivalent concentrations of [SO_4^{2-} + NO_3^-] were much higher than those of [NH_4^+], suggesting that NH_4^+ was not enough to be neutralized with NO_3^-, and therefore, a part of NO_3^- was present in other forms, such as KNO_3 and $Ca(NO_3)_2$. This might be true since

https://doi.org/10.1021/acs.est.1c03957
Environ. Sci. Technol. 2021, 55, 12261−12271

NO_3^- correlated well with K^+ and Ca^{2+} ($r > 0.53$, $p < 0.05$, see Figure S5), especially during the springtime. In the atmosphere, K^+ mainly originated from both crustal and BB emissions.[47,48] Due to a poor correlation between K^+ and Ca^{2+} (a tracer of dust, Figure S6), we suggested that K^+ at QOMS was mainly from BB emission. The primary particles from BB possessed NO_3^-/K^+ ratios in the range of 0.02−0.13,[49] while particulates derived from fugitive dust exhibited NO_3^-/Ca^{2+} ratios ranging from 0.02 to 0.09.[50] At QOMS, the average NO_3^-/K^+ and NO_3^-/Ca^{2+} ratios were 13.8 ± 7.7 and 1.1 ± 1.4, respectively, which were 1−2 orders of magnitude higher than those of the primary particles emitted from BB and dust, implying that nitrate at QOMS was mostly from secondary transformation. At QOMS, the seasonal variations in the NO_3^- concentration mimicked that of TWSIIs, with the highest level in the springtime (0.9 $\mu g\ m^{-3}$) and the lowest one in the summertime (0.3 $\mu g\ m^{-3}$, see Table S2). The intensive BB-emitted pollution over the South Asian continent could explain the increased NO_3^- concentrations in the springtime. The enhanced K^+ concentrations and a highly good correlation between NO_3^- and K^+ (r = 0.84) in the springtime also supported this argument (Figure S5).

Nitrogen and Oxygen Isotope Ratios. The time series of $\delta^{15}N\text{-}NO_3^-$, $\delta^{18}O\text{-}NO_3^-$, and $\Delta^{17}O\text{-}NO_3^-$ values in TSP at QOMS are plotted in Figure 1b−d. Except for those during the heavy precipitation events, most of the aerosol samples were analyzed for nitrogen and oxygen isotopes. The $\delta^{15}N\text{-}NO_3^-$ values varied from −7.8 to 17.1‰ with a mean value of 0.4 ± 4.9‰. This value was higher than those at Mt. Lulin (2862 m a.s.l., Taiwan, −3.6‰) and QOMS (−5.1‰) of 2018 spring and summer, but were much lower than those in urban cities (from 0.8‰ in Chengdu to 10.9‰ in Nanjing, see Figure 3a). Airborne nitrate aerosols were mainly produced by the secondary transformation from their precursor, NO_x, which exhibited the unique $\delta^{15}N\text{-}NO_x$ signatures from its different emissions. As shown in Figure 3b, NO_x from coal combustion possessed higher $\delta^{15}N\text{-}NO_x$ values, and therefore, the lower $\delta^{15}N\text{-}NO_3^-$ values in this work reflected lower contributions of coal combustion to nitrate aerosols compared to those Chinese cities.[27] The average $\delta^{15}N\text{-}NO_3^-$ values in the different seasons are listed in Table S2. The highest $\delta^{15}N\text{-}NO_3^-$ value (8.0 ± 5.8‰) was observed in the autumn, whereas the lowest one (−2.1 ± 2.2‰) was found in the summer. Coal combustion possessed higher $\delta^{15}N\text{-}NO_x$ values (+9 to +18‰) compared to the biogenic soil emission (−43 to −22‰). Consequently, the higher $\delta^{15}N\text{-}NO_3^-$ values in autumn suggested that the higher relative contribution of coal combustion to nitrate aerosols. The depleted $\delta^{15}N\text{-}NO_3^-$ values in summer might be associated with the higher proportion of biogenic soil emission to nitrate aerosols; this will be discussed in the Source Apportionments of Nitrate section.

In terms of oxygen isotopic compositions, the $\delta^{18}O\text{-}NO_3^-$ values ranged from 43.6 to 96.2‰ at QOMS, with an average value of 64.7 ± 11.5‰. The $\Delta^{17}O\text{-}NO_3^-$ values varied from 5.0 to 39.2‰ with a mean value of 27.6 ± 6.9‰. The fluctuations in the $\delta^{18}O\text{-}NO_3^-$ and $\Delta^{17}O\text{-}NO_3^-$ values of the daily nitrate aerosol samples were attributed to the differences in relative contributions of OH and N_2O_5 pathways to nitrate formation.[10,11,51] At QOMS, the average $\Delta^{17}O\text{-}NO_3^-$ value was 27.6‰, which was in agreement with those in Shanghai (25.6‰, see Figure 3c) and QOMS of 2018 spring and summer.[14,52] Our $\Delta^{17}O\text{-}NO_3^-$ value was also similar to that in Beijing (26.3‰) where hydrolysis of N_2O_5 was a major formation mechanism of nitrate due to the high N_2O_5 concentrations and aerosol loadings, especially on polluted days.[10,53] Nevertheless, the $\Delta^{17}O\text{-}NO_3^-$ value at Mt. Lulin (17.0‰) was much lower than that at QOMS,[51] probably suggesting that more OH oxidation pathway to nitrate production existed at Mt. Lulin since it is located in the subtropical free troposphere.

The significant seasonal variations of $\delta^{18}O\text{-}NO_3^-$ and $\Delta^{17}O\text{-}NO_3^-$ values were also found at QOMS. As listed in Table S2, the average $\Delta^{17}O\text{-}NO_3^-$ ($\delta^{18}O\text{-}NO_3^-$) values in the spring, summer, autumn, and winter were 29.8 ± 4.7‰ (66.0 ± 10.6‰), 20.2 ± 7.0‰ (51.6 ± 11.8‰), 18.8 ± 8.8‰ (59.4 ± 12.5‰), and 25.6 ± 7.1% (66.2 ± 12.1‰), respectively. Both $\delta^{18}O\text{-}NO_3^-$ and $\Delta^{17}O\text{-}NO_3^-$ showed higher values in the spring and winter, whereas lower values were found in the summer and autumn. The depletion of $\delta^{18}O\text{-}NO_3^-$ and $\Delta^{17}O\text{-}NO_3^-$ values in the summer can be interpreted by the higher proportion of NO_2 + OH to nitrate formation at high OH radical concentrations due to stronger photochemical reactions in the hot season. In contrast, more nitrate aerosols were formed by the heterogeneous processes, resulting in enriched $\delta^{18}O\text{-}NO_3^-$ and $\Delta^{17}O\text{-}NO_3^-$ values in the springtime and wintertime.

Potential Formation Pathways of Nitrate Aerosols. Previous studies have suggested that $\Delta^{17}O$ was more appropriate to discriminate nitrate production via OH and N_2O_5 pathways than $\delta^{18}O$ because of the distinct $\delta^{18}O$ values in different O sources.[54,55] In this section, we attempted to quantify the formation pathways of nitrate aerosols at QOMS using the $\Delta^{17}O$ approach. Assuming that the atmospheric nitrate aerosols were mainly produced by NO_2 + OH (R_1), N_2O_5 + H_2O (R_2), and NO_3 + HC/DMS (R_3), the observed $\Delta^{17}O\text{-}NO_3^-$ in TSP ambient samples ($[\Delta^{17}O\text{-}NO_3^-]_{TSP}$) should be satisfied with

$$[\Delta^{17}O - NO_3^-]_{TSP} = [\Delta^{17}O - NO_3^-]_{R1}\cdot f_{R1} + [\Delta^{17}O - NO_3^-]_{R2}\cdot f_{R2} + [\Delta^{17}O - NO_3^-]_{R3}\cdot f_{R3} \quad (1)$$

and $f_{R1} + f_{R2} + f_{R3} = 1$. In eq 1, f_{R1}, f_{R2}, and f_{R3} are the relative fractions of NO_2 + OH, N_2O_5 + H_2O, and NO_3 + HC/DMS for nitrate production. $[\Delta^{17}O\text{-}NO_3^-]_{R1}$, $[\Delta^{17}O\text{-}NO_3^-]_{R2}$, and $[\Delta^{17}O\text{-}NO_3^-]_{R3}$ are the $\Delta^{17}O\text{-}NO_3^-$ values produced by NO_2 + OH, N_2O_5 + H_2O, and NO_3 + HC/DMS reactions, respectively, and the endmembers of $\Delta^{17}O\text{-}NO_3^-$ values for the three different mechanisms can be calculated as[54]

$$[\Delta^{17}O - NO_3^-]_{R1}\ (‰) = 2/3\alpha\cdot\Delta^{17}O(O_3^*) \quad (2)$$

$$[\Delta^{17}O - NO_3^-]_{R2}\ (‰) = 1/2\ (2/3\alpha\cdot\Delta^{17}O(O_3^*) + 1/3\cdot\Delta^{17}O(O_3^*)) + 1/3\alpha\cdot\Delta^{17}O(O_3^*) \quad (3)$$

$$[\Delta^{17}O - NO_3^-]_{R3}\ (‰) = 2/3\alpha\cdot\Delta^{17}O(O_3^*) + 1/3\cdot\Delta^{17}O(O_3^*) \quad (4)$$

where α is the mole fraction of NO that is oxidized by O_3 and can be calculated from the observations of NO, O_3, HO_2, and RO_2 concentrations.[10,52] $\Delta^{17}O(O_3^*)$ is the $\Delta^{17}O$ value of the terminal oxygen atoms of O_3 and can be estimated by $\Delta^{17}O$ values in bulk ozone (average value: ∼25.9‰) by multiplying

https://doi.org/10.1021/acs.est.1c03957
Environ. Sci. Technol. 2021, 55, 12261−12271

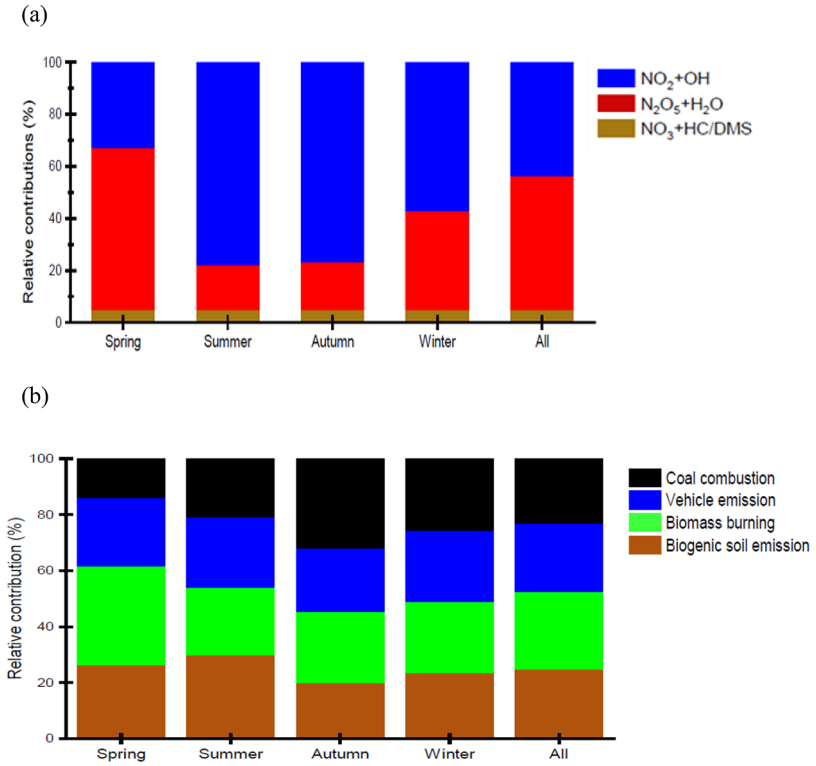

Figure 4. Seasonal variations of the relative contributions of various (a) formation pathways and (b) emission sources to nitrate aerosols at QOMS during the sampling periods.

with a factor of 1.5.[56−58] During the sampling period, the concentrations of NO, O_3, HO_2, and RO_2 were not measured, hence the α values were obtained from the literature studies[10,52,56,57] ranging from 0.6 to 0.8 for the gas-phase oxidation (R_1) and 1.0 for nocturnal chemistry ($R_2 + R_3$) of nitrate production, which were appropriately used for the estimation of the endmember of $\Delta^{17}O\text{-}NO_3^-$ values for the three different formation pathways of nitrate at the remote background site.[58,59] Using these α values, the endmembers of $[\Delta^{17}O\text{-}NO_3^-]_{R1}$ (α = 0.6, 15.5‰; 0.7, 18.1‰; 0.8, 20.7‰), $[\Delta^{17}O\text{-}NO_3^-]_{R2}$ (32.4‰), and $[\Delta^{17}O\text{-}NO_3^-]_{R3}$ (38.9‰) were calculated. The f_{R3} value was in a range of 0.05−0.25 from the global means to that in the polluted Beijing.[4,60] Then, the formation pathways can be quantified using eq 1.

As listed in Table S3, the assumptions of α values and f_{R3} did influence the partitions of formation mechanisms of nitrate. The average proportions of NO_2 + OH (N_2O_5 + H_2O) to nitrate aerosols were 39% (56%), 43% (52%), and 50% (45%), respectively, when the α values were assumed to be 0.6, 0.7, and 0.8. This indicated that the uncertainty of the different partitioned pathways of nitrate production via α values was better than 16% (e.g., (50 − 43%)/43%). On the contrary, the relative fractions of NO_2 + OH (N_2O_5 + H_2O) to nitrate were, respectively, 43% (52%), 42% (43%). and 40% (35%) as the f_{R3} values were assumed to be 0.05, 0.15, and 0.25 with an α value of 0.7. The increase in f_{R3} decreased the relative fraction of N_2O_5 + H_2O to nitrate production with an uncertainty of 33% (e.g., (52 − 35%)/52%). Irrespective of the α and f_{R3} values we used, our results reflected that the nocturnal chemistry ($R_2 + R_3$) was an important pathway for nitrate formation. QOMS is located in a pristine and high mountain area and the concentrations of HC/DMS should be lower than those in polluted cities. Thus, the f_{R3} value was assumed to be 0.05 with α = 0.7 for further estimation of nitrate formation mechanisms for each aerosol sample.

The imbalance of sample numbers between the spring and other seasons might influence the reality of estimated results. Thus, we calculated the average f_{R1} and f_{R2} values in the springtime with two different scenarios for comparison. In scenario I, the average f_{R1} and f_{R2} values were obtained from the estimated results in all spring samples. In scenario II, we selected the springtime $\Delta^{17}O\text{-}NO_3^-$ data, which followed the regular sampling frequency (7 days since March 23, 2017, the first sampling date) for quantification of nitrate formation pathways and then calculated the average f_{R1} and f_{R2} values. By our statistics, the average $\Delta^{17}O\text{-}NO_3^-$ value in the springtime of scenario I was 29.80‰ (19.47−39.26‰), which was close to that of scenario II (31.07, 19.57−35.16‰). Figure S7a reveals the estimated formation pathways of nitrate in the springtime for the two different scenarios. As can be seen, the calculated results of the two scenarios were in agreement, suggesting that the different sampling numbers in the springtime did not influence the estimated results in our case. Consequently, we used the estimated results from scenario I for the following discussion. As shown in Figure 4a, the relative contributions of NO_2 + OH and N_2O_5 + H_2O to nitrate aerosols (f_{R3} = 0.05, α = 0.7 for gas-phase oxidation) were, on average, 43 and 52%, respectively. Hydrolysis of N_2O_5 predominated for nitrate production in the springtime with a fraction of 62%. The high proportion of N_2O_5 + H_2O might be attributed to the spring-maximum O_3 concentrations in the HTP region,[61−63] which was favorable for N_2O_5 oxidation pathways. On the contrary, NO_2 + OH was a dominant oxidation pathway of NO_x to NO_3^- in the summer (78%). A higher fraction of NO_2 + OH in the summer was expected since high temperature and stronger solar radiation facilitated

https://doi.org/10.1021/acs.est.1c03957
Environ. Sci. Technol. 2021, 55, 12261−12271

the nitrate formation by gas-phase oxidation. The dominance of NO_2 + OH to nitrate production was also found in the autumn (~77%). This value was in line with that (NO_2 + OH contributed ~72% to nitrate) at QOMS in the 2018 fall season,[14] implying that the nitrate aerosols at QOMS in the autumn were mainly contributed by the NO_2 + OH reaction. In addition, the contribution of N_2O_5 + H_2O to NO_3^- increased from 14% in the low-NO_3^- level (NO_3^- <0.3 $\mu g\ m^{-3}$) to 85% when the NO_3^- concentration was higher than 3 $\mu g\ m^{-3}$ (see Figure S8). This reflected that hydrolysis of N_2O_5 played an important role in nitrate production at QOMS, especially in the high-NO_3^--level events.

Source Apportionments of Nitrate. Nitrogen isotopic composition enables tracking potential sources of nitrate aerosols.[6,9] One caution has to be made, that is, the fractionation effects on $\delta^{15}N$ during the conversion of NO_x to NO_3^- cannot be neglected.[32,55] In this section, we used the $\delta^{15}N$-NO_3^- values along with the SIAR model to quantify the potential sources of nitrate aerosols at QOMS. Before that, the fractionation factors of $\delta^{15}N$ from NO_x to NO_3^- had to be estimated. The detailed calculation approach of fractionation factors of $\delta^{15}N$ from NO_x to NO_3^- can be found in Supporting Information S3; the relevant parameters used in this approach are listed in Table S4. As shown in Figure S9, the fractionation factor of $\delta^{15}N$ for each aerosol sample varied from 5.9 to 8.1‰ with a mean value of 7.3 ± 0.5‰. Due to the increases of $\delta^{15}N$ values from NO_x to NO_3^-, the corresponding fractionation factor had to be subtracted from $\delta^{15}N$-NO_3^- in each TSP sample to eliminate the fractionation effects of $\delta^{15}N$-NO_3^- prior to estimating the source apportionments of nitrate aerosols.[6] Coal combustion, vehicle emission, biomass burning, and biogenic soil emission were considered to be the important sources of nitrate aerosols in the estimation. Since the SIAR model worked well for numerous data sets ($N \geq 10$),[28] the $\delta^{15}N$-NO_3^- data collected in the same season would serve as one input for this model to resolve the source apportionments of nitrate at QOMS. Again, we also estimated the source apportionments of nitrate aerosols in the springtime by the SIAR model for two different scenarios. In scenario I, we used all of the observed $\delta^{15}N$-NO_3^- data in the spring to serve as input. In scenario II, the spring $\delta^{15}N$-NO_3^- data, which followed the regular sampling frequency at QOMS (7 days since March 23, 2017), served as input in the SIAR model. The results showed that the average $\delta^{15}N$-NO_3^- values in the springtime of scenarios I and II were −0.96 ± 3.24‰ (−7.74 to 5.44‰) and −0.99 ± 4.35‰ (−7.03 to 5.44‰), respectively, suggesting an insignificant difference. Although a slight difference in the relative contributions of BB to nitrate (35 vs 32%, Figure S7b) was observed in the two different scenarios, both results highlighted that BB was the predominant source of nitrate in the springtime. Thus, we finally used the scenario-I-simulated results to investigate the potential sources of nitrate in the springtime and also compared them with those in other seasons.

During the sampling period, BB activities were the predominant source to NO_3^- aerosols at QOMS, accounting for 28 ± 5%, followed by biogenic soil emission (25 ± 4%), vehicle emission (24 ± 1%), and coal combustion (23 ± 8%, Figure 4b). On average, the ratio of fossil-fuel-derived (coal combustion + vehicle emission) nitrate to non-fossil-fuel-produced (biomass burning + biogenic soil emission) nitrate was approximately 1.0. Our value was much lower than those in Chinese megacities (from 1.17 in Chengdu to 1.81 in Beijing), where the combustion of fossil fuel was a dominant emission source of nitrate aerosols.[27]

Except for traffic emission, the relative contributions of other sources to nitrate exhibited apparent seasonal distributions. The relative contribution of BB to nitrate in the springtime was 35%, exceeding those in other seasons (24−25%) by factors of 1.4−1.5. As shown in Figure 2a, intensive fire spots were observed in South Asia, and the air parcels spent much time staying in northern India and Nepal, picking up the BB pollution, transporting to the receptor site, and resulting in enhancements of nitrate aerosols. High K^+ concentrations in the springtime also supported our arguments. On the other hand, we found that BB also contributed partly to nitrate in the summer. This might be true since yak dung was regularly burnt for residential cooking and heating in the HTP region all year round, of course, including the summer season.[64] For coal combustion, its contribution revealed the highest value in the autumn (32%). This did contradict with the maximum coal consumption patterns in winter over China. At QOMS, northern India and Nepal were the major source regions of atmospheric aerosols. A previous study has shown that the concentrations of coal-combusted air pollutants (from India) in northern India were regularly highest during the autumn season driven by the Indian monsoon.[65] This might explain the highest contribution of coal combustion to nitrate in the autumn since northern India was a major source region of aerosols at QOMS. The relative contributions of biogenic soil emission were maximum in the summer with a contribution of 30%. This was expected since more NO_x from biogenic soil emission was released into the atmosphere under the high soil temperature (ambient temperature: ~11 °C) conditions.[66]

Wang et al.[14] determined $\Delta^{17}O$-NO_3^- and $\delta^{15}N$-NO_3^- values in TSP samples at QOMS from April to September 2018. Figure S10 shows the comparisons of $\delta^{15}N$-NO_3^- and $\Delta^{17}O$-NO_3^- values between the two studies. Compared to 2017, the lower $\delta^{15}N$-NO_3^- values were found in both seasons of 2018, suggesting that the different emission sources might alternate the $\delta^{15}N$-NO_3^- values at QOMS in different years. In December 2017, the Indian government required installation of low NO_x burners and over-fired air in addition to the selective catalytic reduction in coal-fired power plants, in order to reduce the NO_x emissions. Since then, these power plants started to implement these control measures one after another in India.[67,68] Thus, the decrease of NO_x emissions from the coal-fired power plants in India after 2018 might explain the lower average $\delta^{15}N$-NO_3^- values at QOMS. However, the $\Delta^{17}O$-NO_3^- values in 2017 were close to those in 2018, suggesting similar formation pathways of nitrate aerosols.

In this work, we used the Monte Carlo approach in the SIAR model to identify the emission sources of nitrate aerosols at QOMS. Using the SIAR model, the number of emission sources serving as input would influence the modeled results. A strong negative correlation of probability density function (PDF) between two different sources indicated that the model was unable to completely differentiate one source from another.[28] Figure S11 shows an example of the PDF of each emission source to nitrate when three or four emission sources were considered. The results indicated that the PDF of each source revealed normal distributions. In addition, we found that the correlation coefficients of PDF between coal combustion (vehicle emission) and biomass burning decreased significantly when the number of emission sources increased. This implied that the inter-influence between coal combustion

https://doi.org/10.1021/acs.est.1c03957
Environ. Sci. Technol. 2021, 55, 12261−12271

(vehicle emission) and biomass burning reduced significantly when we considered four emission sources in the SIAR model. However, the relative contributions of coal combustion showed a moderate correlation ($r = -0.63$) with that of BB emission, suggesting that misclassification between two sources. Thus, we highlighted that more measurements of δ^{15}N-NO_x from various emission sources for improvements of quantification in emission sources to nitrate will be needed in the future.

■ ASSOCIATED CONTENT

Supporting Information

The Supporting Information is available free of charge at https://pubs.acs.org/doi/10.1021/acs.est.1c03957.

Calculation of Δ^{17}O; SIAR model theory; estimation of fractionation factors; δ^{15}N-NO_x values in emission sources; seasonal variations of isotope values; nitrate formation pathways with different α and f_{R3}; air clusters; the correlation between species; formation pathways and sources in different scenarios; estimated fractionation factors; isotope ratio comparison with literature studies; PDF function in the SIAR model (PDF)

■ AUTHOR INFORMATION

Corresponding Author

Yan-Lin Zhang − *Yale-NUIST Center on Atmospheric Environment, International Joint Laboratory on Climate and Environment Change, Nanjing University of Information Science and Technology, Nanjing 210044, China; Key Laboratory Meteorological Disaster, Ministry of Education & Collaborative Innovation Center on Forecast and Evaluation of Meteorological Disaster, Nanjing University of Information Science and Technology, Nanjing 210044, China; Jiangsu Provincial Key Laboratory of Agricultural Meteorology, School of Applied Meteorology, Nanjing University of Information Science & Technology, Nanjing 210044, China;* orcid.org/0000-0002-8722-8635; Email: dryanlinzhang@outlook.com, zhangyanlin@nuist.edu.cn

Authors

Yu-Chi Lin − *Yale-NUIST Center on Atmospheric Environment, International Joint Laboratory on Climate and Environment Change, Nanjing University of Information Science and Technology, Nanjing 210044, China; Key Laboratory Meteorological Disaster, Ministry of Education & Collaborative Innovation Center on Forecast and Evaluation of Meteorological Disaster, Nanjing University of Information Science and Technology, Nanjing 210044, China; Jiangsu Provincial Key Laboratory of Agricultural Meteorology, School of Applied Meteorology, Nanjing University of Information Science & Technology, Nanjing 210044, China;* orcid.org/0000-0003-4227-8978

Mingyuan Yu − *Yale-NUIST Center on Atmospheric Environment, International Joint Laboratory on Climate and Environment Change, Nanjing University of Information Science and Technology, Nanjing 210044, China; Key Laboratory Meteorological Disaster, Ministry of Education & Collaborative Innovation Center on Forecast and Evaluation of Meteorological Disaster, Nanjing University of Information Science and Technology, Nanjing 210044, China; Jiangsu Provincial Key Laboratory of Agricultural Meteorology, School of Applied Meteorology, Nanjing University of Information Science & Technology, Nanjing 210044, China*

Mei-Yi Fan − *Yale-NUIST Center on Atmospheric Environment, International Joint Laboratory on Climate and Environment Change, Nanjing University of Information Science and Technology, Nanjing 210044, China; Key Laboratory Meteorological Disaster, Ministry of Education & Collaborative Innovation Center on Forecast and Evaluation of Meteorological Disaster, Nanjing University of Information Science and Technology, Nanjing 210044, China; Jiangsu Provincial Key Laboratory of Agricultural Meteorology, School of Applied Meteorology, Nanjing University of Information Science & Technology, Nanjing 210044, China;* orcid.org/0000-0002-3311-8799

Feng Xie − *Yale-NUIST Center on Atmospheric Environment, International Joint Laboratory on Climate and Environment Change, Nanjing University of Information Science and Technology, Nanjing 210044, China; Key Laboratory Meteorological Disaster, Ministry of Education & Collaborative Innovation Center on Forecast and Evaluation of Meteorological Disaster, Nanjing University of Information Science and Technology, Nanjing 210044, China; Jiangsu Provincial Key Laboratory of Agricultural Meteorology, School of Applied Meteorology, Nanjing University of Information Science & Technology, Nanjing 210044, China*

Wen-Qi Zhang − *Yale-NUIST Center on Atmospheric Environment, International Joint Laboratory on Climate and Environment Change, Nanjing University of Information Science and Technology, Nanjing 210044, China; Key Laboratory Meteorological Disaster, Ministry of Education & Collaborative Innovation Center on Forecast and Evaluation of Meteorological Disaster, Nanjing University of Information Science and Technology, Nanjing 210044, China; Jiangsu Provincial Key Laboratory of Agricultural Meteorology, School of Applied Meteorology, Nanjing University of Information Science & Technology, Nanjing 210044, China*

Guangming Wu − *Institute of Tibetan Plateau Research, Chinese Academy of Sciences, Beijing 100101, China;* orcid.org/0000-0002-7043-8169

Zhiyuan Cong − *Institute of Tibetan Plateau Research, Chinese Academy of Sciences, Beijing 100101, China;* orcid.org/0000-0002-7545-5611

Greg Michalski − *Department of Earth, Atmospheric, and Planetary Sciences and Department of Chemistry, Purdue University, West Lafayette, Indiana 47907, United States*

Complete contact information is available at: https://pubs.acs.org/10.1021/acs.est.1c03957

Notes

The authors declare no competing financial interest.

■ ACKNOWLEDGMENTS

This study was financially supported by the Natural Scientific Foundation of China (no. 41977305), the Provincial Natural Science Foundation of Jiangsu (Grant no. BK20180040), and the Jiangsu Innovation & Entrepreneurship Team. The authors would like to thank the QOMS station for providing the meteorological data in this study.

REFERENCES

(1) Xue, H.; Feingold, G. A modeling study of the effect of nitric acid on cloud properties. *J. Geophys. Res.: Atmos.* **2004**, *109*, No. D18204.

(2) Makkonen, R.; Romakkaniemi, S.; Kokkola, H.; Stier, P.; Räisänen, P.; Rast, S.; Feichetr, J.; Kulmala, M.; Laaksonen, A. Brightening of the global cloud filed by nitric acid and the associated radiative forcing. *Atmos. Chem. Phys.* **2012**, *12*, 7625−7633.

(3) Brown, S. S.; Stutz, J. Nighttime radical observation and chemistry. *Chem. Soc. Rev.* **2012**, *41*, 6405−6447.

(4) Alexander, B.; Sherwen, T.; Holmes, C. D.; Fisher, J. A.; Chen, Q.; Evans, M. J.; Kasibhatla, P. Global inorganic nitrate production mechanisms: comparison of a global model with nitrate isotope observations. *Atmos. Chem. Phys.* **2020**, *20*, 3859−3877.

(5) Dao, X.; Lin, Y.-C.; Cao, F.; Di, S.-Y.; Hong, Y.; Xin, G.; Li, G.; Fu, P.; Zhang, Y.-L. Introduction to the national aerosol chemical composition monitoring network of China: objectives, current status and outlook. *Bull. Am. Meteorol. Soc.* **2019**, *100*, ES337−ES351.

(6) Fan, M.-Y.; Zhang, Y.-L.; Lin, Y.-C.; Cao, F.; Zhao, X.-Y.; Sun, Y.; Qiu, Y.; Fu, P.; Wang, Y. Changes of emission sources to nitrate aerosols in Beijing after the clean air action: evidence from dual isotope compositions. *J. Geophys. Res.: Atmos.* **2020**, *125*, No. e31998.

(7) Zhao, Z.; Cao, J.; Shen, Z.; Huang, R.-J.; Hu, T.; Wang, P.; Zhang, T.; Liu, S. Chemical composition of PM2.5 at a high-altitude regional background site of Northeast of Tibet Plateau. *Atmos. Pollut. Res.* **2015**, *6*, 815−823.

(8) Zong, Z.; Wang, X.; Tian, C.; Chen, Y.; Fang, Y.; Zhang, F.; Li, C.; Sun, J.; Li, J.; Zhang, G. First assessment of NOx source at a regional background site in northern China using isotopic analysis linked with modeling. *Environ. Sci. Technol.* **2017**, *51*, 5923−5931.

(9) Chang, Y.; Zhang, Y.; Tian, C.; Zhang, S.; Ma, X.; Cao, F.; Liu, X.; Zhang, W.; Kuhn, T.; Lehmann, M. F. Nitrogen isotope fractionation during gas-to-particle conversion of NOx to NO3- in the atmosphere - implications for isotope-based NOx source apportionment. *Atmos. Chem. Phys.* **2018**, *18*, 11647−11661.

(10) He, P.; Xie, Z.; Chi, X.; Yu, X.; Fan, S.; Kang, H.; Liu, C.; Zhan, H. Atmospheric Δ17(NO3-) reveals nocturnal chemistry dominates nitrate production in Beijing haze. *Atmos. Chem. Phys.* **2018**, *18*, 14465−14476.

(11) Michalski, G.; Scott, Z.; Kabiling, M.; Thiemens, M. H. First measurements and modeling of Δ17O in atmospheric nitrate. *Geophys. Res. Lett.* **2003**, *30*, No. 1870.

(12) Hastings, M. G.; Sigman, D. M.; Lipschultz, F. Isotopic evidence for source changes of nitrate in rain at Bermuda. *J. Geophys. Res.: Atmos.* **2003**, *108*, No. 4790.

(13) Luo, L.; Pan, Y.-Y.; Zhu, R.-G.; Zhang, Z.-Y.; Zheng, N.-J.; Liu, Y.-H.; Liu, C.; Xiao, H.-W.; Xiao, H.-Y. Assessment of the seasonal cycle of nitrate in PM2.5 using chemical compositions and stable nitrogen and oxygen isotopes at Nanchang, China. *Atmos. Environ.* **2020**, *225*, No. 117371.

(14) Wang, K.; Hattori, S.; Kang, S.; Lin, M.; Yoshida, N. Isotopic constrains on the formation pathways and sources of atmospheric nitrate in the Mt. Everest region. *Environ. Pollut.* **2020**, *267*, No. 115274.

(15) Chen, X.; Kang, S.; Cong, Z.; Yang, J.; Ma, Y. Concentration, temporal variation, and sources of black carbon in the Mt. Everest region retrieved by real-time observation and simulation. *Atmos. Chem. Phys.* **2018**, *18*, 12859−12875.

(16) Xu, J. Z.; Zhang, Q.; Wang, Z. B.; Yu, G. M.; Ge, X. L.; Qin, X. Chemical composition and size distribution of summertime PM2.5 at a high altitude remote location in the northeast of the Qinghai-Xizang (Tibet) Plateau: insight into aerosol sources and processing in free troposphere. *Atmos. Chem. Phys.* **2015**, *15*, 5069−5081.

(17) Niu, H.; Kang, S.; Wang, H.; Zhang, R.; Lu, X.; Qian, Y.; Paudyal, R.; Wang, S.; Shi, X.; Yan, X. Seasonal variation and light absorption property of carbonaceous aerosol in a typical glacier region of the southeast Tibetan Plateau. *Atmos. Chem. Phys.* **2018**, *18*, 6441−6460.

(18) Li, C.; Bosch, C.; Kang, S.; Andersson, A.; Chen, P.; Zhang, Q.; Cong, Z.; Chen, B.; Qin, D.; Gustafsson, Ö. Sources of black carbon to the Himalayan-Tibetan Plateau glaciers. *Nat. Commun.* **2016**, *7*, No. 12574.

(19) Cong, Z.; Kang, S.; Kawamura, K.; Liu, B.; Wang, X.; Wang, Z.; Gao, S.; Fu, P. Carbonaceous aerosols on the south edge of the Tibetan Plateau: concentrations, seasonality and source. *Atmos. Chem. Phys.*, **2015**, *15*, 1573−1584.

(20) Kang, S.; Zhang, Q.; Qian, Y.; Ji, Z.; Li, C.; Cong, Z.; Zhang, Y.; Guo, J.; Du, W.; Huang, J.; You, Q.; Panday, A. K.; Rupakheti, M.; Chen, D.; Gustafsson, Ö.; Thiemens, M. H.; Qin, D. Liking atmospheric pollution to cryospheric change in the Third Pole region: current progress and future prospects. *Natl. Sci. Rev.* **2019**, *6*, 796−809.

(21) Ma, Y.; Wang, Y.; Zhong, L.; Wu, R.; Wang, S.; Li, M. The characteristics of atmospheric turbulence and radiation energy transfer and the structure of atmospheric boundary layer over the northern slop area of Himalaya. *J. Meteorol. Soc. Jpn.* **2011**, *89A*, 345−353.

(22) Fan, M.-Y.; Zhang, Y.-L.; Lin, Y.-C.; Chang, Y.-H.; Cao, F.; Zhang, W.-Q.; Hu, Y.-B.; Bao, M.-Y.; Liu, X.-Y.; Zhai, X.-Y.; Lin, X.; Zhao, Z.-Y.; Song, W.-H. Isotope-based source apportionment of nitrogen-containing aerosols: a case study in an industrial city in China. *Atmos. Environ.* **2019**, *212*, 96−105.

(23) Sigman, D. M.; Casciotti, K. L.; Andreani, M.; Barford, C.; Galanter, M.; Böhlke, J. K. A bacteria method for the nitrogen isotopic analysis of nitrate in seawater and freshwater. *Anal. Chem.* **2001**, *73*, 4145−4153.

(24) Casciotti, K. L.; Sigman, D. M.; Hastings, M. G.; Böhlke, J. K.; Hilkert, A. Measurement of the oxygen isotopic composition of nitrate in seawater and freshwater using the denitrifier method. *Anal. Chem.* **2002**, *74*, 4905−4912.

(25) Böhlke, J. K.; Mroczkowski, S. J.; Coplen, T. B. Oxygen isotopes in nitrate: new reference materials for 18O:17O:16O measurements and observations on nitrate water equilibration. *Rapid Commun. Mass Spectrom.* **2003**, *17*, 1835−1846.

(26) Zhao, Z.; Cao, F.; Fan, M.-Y.; Zhang, W.-Q.; Zhai, X.-Y.; Wang, Q.; Zhang, Y.-L. Coal and biomass burning as major emissions of NOx in Northeast China: Implication from dual isotope analysis of fine nitrate aerosols. *Atmos. Environ.* **2020**, *242*, No. 117762.

(27) Zong, Z.; Tan, Y.; Wang, X.; Tian, C.; Li, J.; Fang, Y.; Chen, Y.; Cui, S.; Zhang, G. Dual-modeling-based source apportionment of NOx in five Chinese megacities: providing the isotopic footprint from 2013 to 2014. *Environ. Int.* **2020**, *137*, No. 105592.

(28) Parnell, A. C.; Inger, R.; Bearhop, S.; Jackson, A. L. Source partition using stable isotopes: coping to much variation. *PLoS One* **2010**, *5*, No. e9672.

(29) Felix, J. D.; Elliott, E. M.; Shaw, S. L. Nitrogen isotopic composition of coal-fired power plant NOx: influence of emission controls and implications for global emission inventories. *Environ. Sci. Technol.* **2012**, *46*, 3528−3535.

(30) Healton, T. H. E. 15N/14N ratios of NOx from vehicle engines and coal-fired power stations. *Tellus B* **1990**, *42*, 304−307.

(31) Moore, H. The isotopic composition of ammonia, nitrogen dioxide and nitrate in the atmosphere. *Atmos. Environ.* **1977**, *11*, 1239−1243.

(32) Walters, W. W.; Goodwin, S. R.; Michalski, G. Nitrogen isotope composition (δ15N) of vehicle emitted-NOx. *Environ. Sci. Technol.* **2015**, *49*, 2278−2285.

(33) Walters, W. W.; Tharp, B. D.; Fang, H.; Hozak, B. J.; Michalski, G. Nitrogen isotope composition of thermally produced NOx from various from fossil-fuel combustion sources. *Environ. Sci. Technol.* **2015**, *49*, 11363−11371.

(34) Fibiger, D. L.; Hasting, M. G.; Lew, A. F.; Peltier, R. E. Collection of NO and NO2 for isotopic analysis of NOx emissions. *Anal. Chem.* **2014**, *86*, 12115−12121.

(35) Fibiger, D. L.; Hastings, M. G. First measurements of the nitrogen isotopic composition of NOx from biomass burning. *Environ. Sci. Technol.* **2016**, *50*, 11569−11574.

https://doi.org/10.1021/acs.est.1c03957
Environ. Sci. Technol. 2021, 55, 12261−12271

(36) Chai, J.; Miller, D. J.; Scheuer, E.; Dibb, J.; Selimovic, V.; Yokelson, R.; Zarzana, K. J.; Brown, S. S.; Koss, A. R.; Warneke, C.; Hastings, M. Isotopic characterization of nitrogen oxides (NOx), nitrous acid (HONO), and nitrate (pNO3-) from laboratory biomass burning during FIREX. *Atmos. Meas. Tech.* **2019**, *12*, 6303−6317.
(37) Miller, D.; Chai, J.; Guo, F.; Dell, C. J.; Karsten, H.; Hastings, M. G. Isotopic composition of in situ soil NOx emissions manure-fertilized cropland. *Geophys. Res. Lett.* **2018**, *45*, 12058−12066.
(38) Li, D.; Wang, X. Nitrogen isotopic signature of soil-release nitric oxide (NO) after fertilizer application. *Atmos. Environ.* **2008**, *42*, 4747−4754.
(39) Felix, J. D.; Elliott, E. M. Isotopic composition of passively collected nitrogen dioxide emission: vehicle, soil and livestock source signatures. *Atmos. Environ.* **2014**, *92*, 359−366.
(40) Ohara, T.; Akimoto, H.; Kurokawa, J.; Horii, N.; Yamaji, N.; Yan, X.; Hayasaka, T. An Asian emission inventory of anthropogenic emission sources for the period 1980-2020. *Atmos. Chem. Phys.* **2007**, *7*, 4419−4444.
(41) Zhao, B.; Wang, P.; Ma, J. Z.; Zhu, S.; Pozzer, A.; Li, W. A high-resolution emission inventory of primary pollutants for the Huabei region, China. *Atmos. Chem. Phys.* **2012**, *12*, 481−501.
(42) Draxler, R. R.; Hess, G. D. An overview of the HYSPLIT_4 modeling system for trajectories, dispersion and deposition. *Aust. Meteorol. Mag.* **1998**, *47*, 295−308.
(43) Denzler, B.; Bogdal, C.; Henne, S.; Obrist, D.; Steinbacher, M.; Hungerbühler, K. Inversion approach to validate mercury emissions based on Background air monitoring at the high altitude research station Jungfraujoch (3580 m). *Environ. Sci. Technol.* **2017**, *51*, 2846−2853.
(44) Martinsson, J.; Monteil, G.; Sporre, M. K.; Hansen, A. M. K.; Kristensson, A.; Stenström, K. E.; Swietlicki, E.; Glasius, M. Exploring sources of biogenic secondary aerosol compounds using chemical analysis and the FLEXPART model. *Atmos. Chem. Phys.* **2017**, *17*, 11025−11040.
(45) Wei, L.; Yue, S.; Zhao, W.; Yang, W.; Zhang, Y.; Ren, L.; Han, X.; Guo, Q.; Sun, Y.; Wang, Z. Stable sulfur isotope ratios and chemical compositions of fine aerosols in Beijing, China. *Sci. Total Environ.* **2018**, *633*, 1156−1164.
(46) Pisso, I.; Sollum, E.; Grythe, H.; Kristiansen, N. I.; Cossiani, M.; Eckhardt, S.; Arnold, D.; Morton, D.; Thompson, R. L.; Groot Ewaaftink, C. D.; Evangeliou, N.; Sodemann, H.; Haimberger, L.; Hanne, S.; Brunner, D.; Burkhart, J. F.; Fouilloux, A.; Brioude, J.; Phillipp, A.; Seibert, P.; Syohl, A. The Lagrangian particle dispersion model FLEXPART version 10.4. *Geosci. Model Dev.* **2019**, *12*, 4955−4997.
(47) Watson, J. G.; Chow, J. C.; Houck, J. E. PM2.5 chemical source profiles for vehicle exhaust, vegetative burning, geological material, and coal burning in Northwestern Colorado during 1995. *Chemosphere* **2001**, *43*, 1141−1151.
(48) Zhang, R.; Jing, J.; Tao, J.; Hsu, S.-C.; Wang, G.; Cao, J.; Lee, C. S. L.; Zhu, L.; Chen, Z.; Zhao, Y.; Shen, Z. Chemical characterization and source apportionment of PM2.5 in Beijing: seasonal perspective. *Atmos. Chem. Phys.* **2013**, *13*, 7053−7074.
(49) Chow, J. C.; Watson, J. G.; Kuhns, H.; Etyemezian, V.; Lowenthal, D. H.; Crow, D.; Kohl, S. D.; Engelbrecht, J. P.; Green, M. C. Source profile for industrial, mobile, and area sources in a Big Ben Regional Aerosol Visibility and Observational study. *Chemosphere* **2004**, *54*, 185−208.
(50) Sun, J.; Shen, Z.; Zhang, L.; Lei, Y.; Gong, X.; Zhang, Q.; Zhang, T.; Xu, H.; Cui, S.; Wang, Q.; Cao, J.; Tao, J.; Zhang, N.; Zhang, R. Chemical source profiles of urban fugitive dust PM2.5 samples from 21 cities across China. *Sci. Total Environ.* **2019**, *649*, 1045−1053.
(51) Guha, T.; Lin, C. T.; Bhattacharya, S. K.; Mahajan, A. S.; Ou-Yang, C.-F.; Lan, Y.-P.; Hsu, S. C.; Liang, M.-C. Isotope ratios of nitrate in aerosol samples from Mt. Lulin, a high-altitude station in central Taiwan. *Atmos. Environ.* **2017**, *154*, 53−69.
(52) He, P.; Xie, Z.; Yu, X.; Wang, L.; Kang, H.; Yue, F. The observation of isotopic compositions of atmospheric nitrate in Shanghai China and its application for reactive nitrogen chemistry. *Sci. Total Environ.* **2020**, *714*, No. 136727.
(53) Wang, H.; Lu, K.; Chen, X.; Zhu, Q.; Chen, Q.; Guo, X.; Jiang, M.; Li, X.; Shang, D.; Tan, Z.; Wu, Y.; Wu, Z.; Zou, Q.; Zheng, Y.; Zeng, L.; Zhu, T.; Hu, M.; Zhang, Y. High N2O5 concentrations observed in urban Beijing: implications of a large nitrate formation pathways. *Environ. Sci. Technol. Lett.* **2017**, *4*, 416−420.
(54) Alexander, B.; Hastings, M. G.; Allman, D. J.; Dachs, J.; Thornton, J. A.; Kunasek, S. A. Quantifying atmospheric nitrate formation pathways based on a global model of the oxygen isotopic composition (Δ17O) of atmospheric nitrate. *Atmos. Chem..Phys.* **2009**, *9*, 5043−5056.
(55) Walters, W. W.; Michalski, G. Theoretical calculation of nitrogen isotope equilibrium exchange fractionation factors of various NOy molecules. *Geochim. Cosmochim. Acta* **2015**, *164*, 284−297.
(56) Vicars, W. C.; Bhattacharya, S. K.; Erbland, J.; Savarina, J. Measurements of the 17O-excess (Δ17O) of tropospheric ozone using a nitrite-coated filter. *Rapid Commun. Mass Spectrom.* **2012**, *26*, 1219−1231.
(57) Michalski, G.; Bhattacharya, S. K. The role of symmetry in the mass independent isotope effect in ozone. *Proc. Natl. Acad. Sci. U.S.A.* **2009**, *106*, 5493−5496.
(58) Morin, S.; Savarino, J.; Frey, M. M.; Domine, F.; Jacobi, H.-W.; Kaleschke, L.; Martins, J. M. F. Comprehensive isotope composition of atmospheric nitrate in the Atlantic Ocean boundary layer from 65°S to 79°N. *J. Geophys. Res.: Atmos.* **2009**, *114*, No. D05303.
(59) Morin, S.; Sander, R.; Savarino, J. Simulation of the diurnal variations of the oxygen isotope anomaly (Δ17O) of reactive atmospheric species. *Atmos. Chem. Phys.* **2011**, *11*, 3653−3671.
(60) Wang, Y.-L.; Song, W.; Yang, W.; Sun, S.-C.; Tong, Y.-D.; Wang, X.-M.; Liu, C.-Q.; Bai, Z.-P.; Liu, X.-Y. Influences of atmospheric pollution on the contribution of major oxidation pathways to PM2.5 nitrate formation in Beijing. *J. Geophys. Res.: Atmos.* **2019**, *124*, 4174−4185.
(61) Cristofanelli, P.; Bracci, A.; Sprenger, M.; Marinoni, A.; Bonafè, U.; Calzolari, F.; Duchi, R.; Laj, P.; Pichon, J. M.; Roccato, F.; Venzac, H.; Vuillermoz, Z.; Bonasoni, P. Tropospheric ozone variations at the Climate Nepal Observatory-Pyramid (Himalayas, 5079 m a.s.l.) and influence of deep stratospheric intrusion events. *Atmos. Chem. Phys.* **2010**, *10*, 6537−6549.
(62) Yin, X.; Kang, S.; de Foy, B.; Cong, Z.; Luo, J.; Zhang, L.; Ma, Y.; Zhang, G.; Rupakheti, D.; Zhang, Q. Surface ozone at Nam Co in the inland Tibetan Plateau: variation, synthesis comparison and regional representativeness. *Atmos. Chem. Phys.* **2017**, *17*, 11293−11311.
(63) Li, R.; Zhao, Y.; Zhou, W.; Meng, Y.; Zhang, Z.; Fu, H. Developing a novel hybrid model for the estimation of surface 8 h ozone (O3) across the remote Tibetan Plateau during 2005-2018. *Atmos. Chem. Phys.* **2020**, *20*, 6159−6175.
(64) Chen, P.; Kang, S.; Bai, J.; Sillanpää, M.; Li, C. Yak dung combustion aerosols in the Tibetan Plateau: chemical characteristics and influence on the local atmospheric environment. *Atmos. Res.* **2015**, *156*, 58−66.
(65) Guttikunda, S. K.; Jawahar, P. Atmospheric emissions and pollution from the coal-fired thermal power plants in India. *Atmos. Environ.* **2014**, *92*, 449−460.
(66) Williams, E. J.; Hutchinson, G. L.; Fehsenfeld, F. C. NOx and N2O emissions from soil. *Global Biogeochem. Cycles* **1992**, *6*, 351−388.
(67) Wiatros-Motyka, M. NOx control for high-ash coal-fired power plants in India. *Clean Energy* **2019**, *3*, 24−33.
(68) Pachouri, R.; Saxena, A. K. *Emission Control in Thermal Power Stations: Issues, Challenges, and the Way Forward*; Energy and Resources Institute: New Delhi, India, 2020.

https://doi.org/10.1021/acs.est.1c03957
Environ. Sci. Technol. 2021, 55, 12261−12271